The Structural Basis for Peptidomimetic Inhibition of Eukaryotic Ribonucleotide Reductase: A Conformationally Flexible Pharmacophore†

Hai Xu,‡ James W. Fairman,§ Sanath R. Wijerathna,‡ Nathan R. Kreischer,|| John LaMacchia,§ Elizabeth Helmbrecht,§ Barry S. Cooperman,|| and Chris Dealwis*,‡

Department of Pharmacology, Case School of Medicine, Case Western Reserve University, 10900 Euclid Avenue, Cleveland, Ohio 44106-4965, Department of Biochemistry and Cellular and Molecular Biology, The University of Tennessee, M407 Walters Life Sciences, Knoxville, Tennessee 37996-0840, Department of Chemistry, University of Pennsylvania, Philadelphia, Pennsylvania 19104

Received March 27, 2008

Eukaryotic ribonucleotide reductase (RR) catalyzes nucleoside diphosphate conversion to deoxynucleoside diphosphate. Crucial for rapidly dividing cells, RR is a target for cancer therapy. RR activity requires formation of a complex between subunits R1 and R2 in which the R2 C-terminal peptide binds to R1. Here we report crystal structures of heterocomplexes containing mammalian R2 C-terminal heptapeptide, P7 (Ac−^{1}FTLDADF^{7}) and its peptidomimetic P6 (^{1}Fmoc(Me)PhgLDChaDF^{7}) bound to *Saccharomyces cerevisiae* R1 (ScR1). P7 and P6, both of which inhibit ScRR, each bind at two contiguous sites containing residues that are highly conserved among eukaryotes. Such binding is quite distinct from that reported for prokaryotes. The Fmoc group in P6 peptide makes several hydrophobic interactions that contribute to its enhanced potency in binding to ScR1. Combining all of our results, we observe three distinct conformations for peptide binding to ScR1. These structures provide pharmacophores for designing highly potent nonpeptide class I RR inhibitors.

Introduction

Ribonucleotide reductases (RRs) catalyze the reduction of ribonucleotides to deoxyribonucleotides, essential building blocks required for DNA replication and repair. RRs are divided into three classes, depending upon which metallocofactors are used to initiate radical-based nucleotide reduction. Class Ia RR, found in all eukaryotes and some prokaryotes and viruses, is a hetero-oligomer of α and β subunits,[1] in which the α subunit (R1) contains the catalytic site (C-site) and allosteric sites and at least one β subunit (R2 or R4) contains a stabilized tyrosyl radical that is essential for enzymatic activity.[2,3] The smallest active holoenzyme for Class 1a RRs is a heterotetramer. Mammalian RR (mRR) and *Escherichia coli* RR (EcRR) have the subunit structure $R1_2R2_2$, whereas the subunit structure for *Saccharomyces cerevisiae* RR (ScRR) is $R1_2R2R4$, in which R2 contains the tyrosyl radical and R4 stabilizes a helix containing the iron ligand of R2.[4]

Because of the central role played by RR in maintaining a balanced nucleotide pool during DNA replication and repair, it is a target for anticancer [5,6] and antiviral therapy.[6,7] In 1990, we demonstrated that mRR can be inhibited by competitive binding at the mR1 subunit by the P7 heptapeptide (N-AcFTLDADF), which corresponds to the C-terminus of the R2 subunit.[8] Transfer-NOE NMR studies demonstrated that P7 bound to mR1, adopting a reverse -turn structure for residues 2−5, TLDA.[9,10] These results, and related structure−function[11–13] and modeling[12] studies, based on the then known structure of *E. coli* R2 (EcR2) C-terminal peptide (EcR2pep) bound to *E. coli* R1 (EcR1),[14] led to the notion that P7 C-terminal peptide binding occurs at two contiguous subsites in mR1, denoted F1 (for the N-terminal Phe residue) and F7 (for the C-terminal Phe residue).[12] The F1 subsite, accommodating the N-terminal portion of the peptide, was posited to be broad, shallow, and hydrophobic and not strongly sequence specific, while the F7 subsite, which accommodates the C-terminal portion, was posited to be narrow and deeper, with very high specificity for the ultimate C- terminal residue. Furthermore, specific locations for the F1 and F7 subsites within mR1 were proposed based on homology with the EcR1:EcR2pep complex structure.[14]

The notion of F1 and F7 subsites guided a series of directed minilibrary screening studies having the goal of developing peptide-based inhibitors of mRR with high affinity for mR1.[15] One important result was the identification of the peptidomimetic, ^{1}Fmoc(Me) PhgLDChaDF,^{7} denoted P6, which has a K_i for mR1 dimer of 310 nM, some 8-fold lower than the corresponding value for P7.

Recently, we reported the first structure of an eukaryotic R1, *S. cerevisiae* R1 (ScR1),[16,17] in which the ScR2 C-terminal peptide (ScR2pep) bound to ScR1 at a locus consisting of residues that are highly conserved between yeast, mouse, and human R1s (but not among prokaryotes), suggesting that the mode of R1−R2 binding is conserved among eukaryotes.[12] A nonapeptide derived from the ScR2 C-terminus was used for making the ScR1−ScR2pep complex, although only the last seven amino acid residues could be located in the structure. We also solved the structure of ScR1 in complex with the C-terminal peptide derived from ScR4 (ScR4pep). Here only the last six amino acid residues could be located.[17]

Interestingly, the ScR2 and ScR4 peptides bound slightly differently to ScR1. Furthermore, to our surprise, the mode of ScR2pep binding to ScR1 was markedly different from that previously reported for the EcR2pep−EcR1 complex.[17] Thus, when the ScR1 and EcR1 structures are superposed (see Supporting Information Figure 1), ScR2pep binds essentially

† The atomic coordinates have been deposited with RCSB ID 2ZLF (complex with P7 peptide) and 2ZLG (complex with P6 peptide).

* To whom correspondence should be addressed. Phone: (216) 368 1652. Fax: (216) 368 1300. E-mail: chris.dealwis@case.edu.

‡ Department of Pharmacology, Case School of Medicine, Case Western Reserve University.

§ Department of Biochemistry and Cellular and Molecular Biology, The University of Tennessee.

|| Department of Chemistry, University of Pennsylvania.

[a] Abbreviations: Cha, β-cyclohexylalanine; Fmoc, 9-fluorenylmethoxycarbonyl and Phg, phenylglycine.

10.1021/jm800350u CCC: $40.75
Published on Web 07/09/2008

Scheme 1

P7

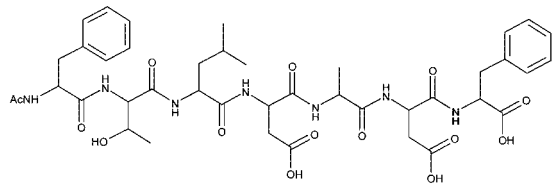

P6

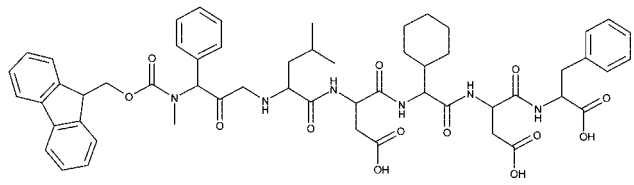

at a right angle with respect to EcR2pep, and in a nonhelical conformation.

The ScR1−ScR2 peptide structure should provide a considerably more reliable model for studying mR1−mR2pep interactions than does our former model based on the EcR1−EcR2pep structure,[12] given the evidence cited above for conservation of R1−R2 binding in eukaryotes and the much higher sequence identity and similarity (66% and 83%, respectively) between human R1 (hR1) and ScR1 as compared with hR1 and EcR1 (29% and 53%, respectively).[12] To test this proposition, we report below the X-ray crystal structures of the mammalian P7 (7 C-terminal residues of mR2pep) and P6 inhibitors (see Scheme 1) in complex with ScR1, as well as the inhibitory effects of P6 and P7 on ScRR activity.

In accord with our expectations, P7 and P6 have inhibitory activities toward ScRR that are similar to those found with mRR. Moreover, our structures reveal that the overall binding of both P7 and P6 to ScR1 is similar to that seen earlier with the ScR2 peptide,[17] with the N-termini of P6 and P7 binding at a predominantly hydrophobic subsite, denoted subsite A, while the C-termini bind at a partially polar/hydrophobic subsite, denoted subsite B. While subsite A has substantial steric overlap with subsite F1 as defined in our earlier model based, in part, on the EcR1−EcR2pep structure,[14] subsite B is located in a totally different part of the R1 structure due to the orthogonality of eR2pep and ScR2pep binding. Interestingly, the conformations of bound P6 and P7 differ, with P7 binding with a reverse turn between its N- and C-termini, similar to what was found with ScR2pep,[17] whereas P6 binds in a more extended fashion. Combining all of our results, we observe three distinct conformations for peptide binding to ScR1, those adopted by: (i) P7/ScR2pep, (ii) P6, and (iii) ScR4pep.

These results demonstrate first, that the ScR1 surface peptide-binding pocket tolerates conformational flexibility, an advantage for drug design, and second, that the ScR1-mR2 peptide heterocomplexes are reasonable structural models for the mR1−mR2 peptide homocomplex. They also provide pharmacophores for the design of future mRR inhibitors having even higher potency than P6.

Results and Discussion

Comparative Inhibition of mRR and ScRR Activities by P6 and P7. Both P6 and P7 (Scheme 1) are potent inhibitors of mRR and ScRR activities, giving the IC_{50} values summarized in Table 1. P7 inhibits mRR somewhat more strongly than ScRR (8.9 μM vs 31 μM), in accord with an earlier report using a crude ScRR preparation,[11] whereas P6 is nearly equipotent towards mRR or ScRR (1.9 μM vs 2.6 μM). The general similarity in inhibition values toward both enzymes may suggest that the binding of peptide and peptidomimetic inhibitors to ScR1 shown in this work provides a good model for how such inhibitors bind to mR1.

Table 1. IC_{50} Values of the P7 and P6 Inhibitors against mRR and ScRR[a]

peptide	IC_{50} (μM), mRR	IC_{50} μM), ScRR
P7	8.9 ± 0.2	31 ± 1
Fmoc-P6	1.9 ± 0.1	2.6 ± 0.1
ScR2		44[b]
ScR4		30[b]

[a] The IC_{50} values for ScR2 and ScR4 against ScRR are also provided. [b] The IC_{50} values were reported in ref 30.

Overall Structure of ScR1−P7 Complex. The entire P7 peptide was visible in the $2F_o - F_c$ Fourier difference electron density map (Figure 1a). The peptide adopts a nonstandard reverse turn involving residues 2−5 when binding to ScR1. P7 binds ScR1 at the periphery at two surface subsites A and B (Figure 1b,c), orthogonally to and separated by the helix αI. Subsite A is positioned near α13 and αD, and subsite B is positioned near αH (Figure 1d).[17]

Subsite A, consisting of V342, E343, Q386, W389, L393, M721, G722, T725, and F729 (see Supporting Information Table 1), is broad and extremely hydrophobic (Figure 1d) and anchors the side chains of the N-terminal F^1 and L^3 residues. F^1 stacks strongly with W389 of αD and also interacts with V342 of α13 and T725 of αI while L^3 packs edge-to-face with F729 of αI. The highly positively charged surface of subsite B contains residues S691, Q692, K693, I696, K723, S726, M727, and Y730 (Figure 1d). The side chain groups of D^6 and F^7 bind in subsite B with the negative charge of the carboxylate terminal, forming two hydrogen bonds with S691 and Q692 and one long-range ion pair interaction with K723. Another ion pair interaction is formed between D^6 and K693 (Figure 1d). The interior of subsite B is narrow and quite hydrophobic, accommodating the side chain of F^7.

The favorable interactions in subsites A and B explain why a heptapeptide is the minimal length required for strong binding to ScR1 and why decreasing peptide length results in decreased inhibitory activity while lengthening the peptide does not improve affinity.[11] On the other hand, the amino terminal group points towards the solvent region, consistent with extension at the N-terminus having little effect on inhibitory potency.[11]

Structural Comparison of P7 and ScR2 Peptide. The P7 (^{1}FTLDADF^7) and ScR2 (^{1}FTFNEDF^7) C-terminal heptapeptides differ between the third and fifth positions (^{3}LDA^5 in P7 is substituted by ^{3}FNE^5 in ScR2). Compared with the ScR2 peptide, P7 exhibits nearly the same backbone conformation when bound to ScR1 (Figure 1e), superposing with an rmsd of 0.85 Å. The greatest conformational differences between the mouse and yeast peptides occur at the N-termini and at the nonstandard reverse turn located in the middle of the molecules. However, in both peptides, the conserved C-terminal residues Asp and Phe, binding in subsite B, superpose well. In the P7 structure, the nonstandard reverse turn ^{2}TLDA^5 makes more hydrogen bonds than the corresponding ^{2}TFNE^{5}residues in the ScR2 peptide (Figure 1d). The conserved Thr residue is crucial, stabilizing the turn by forming an intramolecular hydrogen bond and several van der Waals contacts. In the P7 complex structure, the T^2 Oγ1 is within hydrogen bonding distance of the respective amides of L^3 and D^4. In contrast, the corresponding T^2 residue of the ScR2 peptide hydrogen bonds with the carboxyl side chain of E^5.

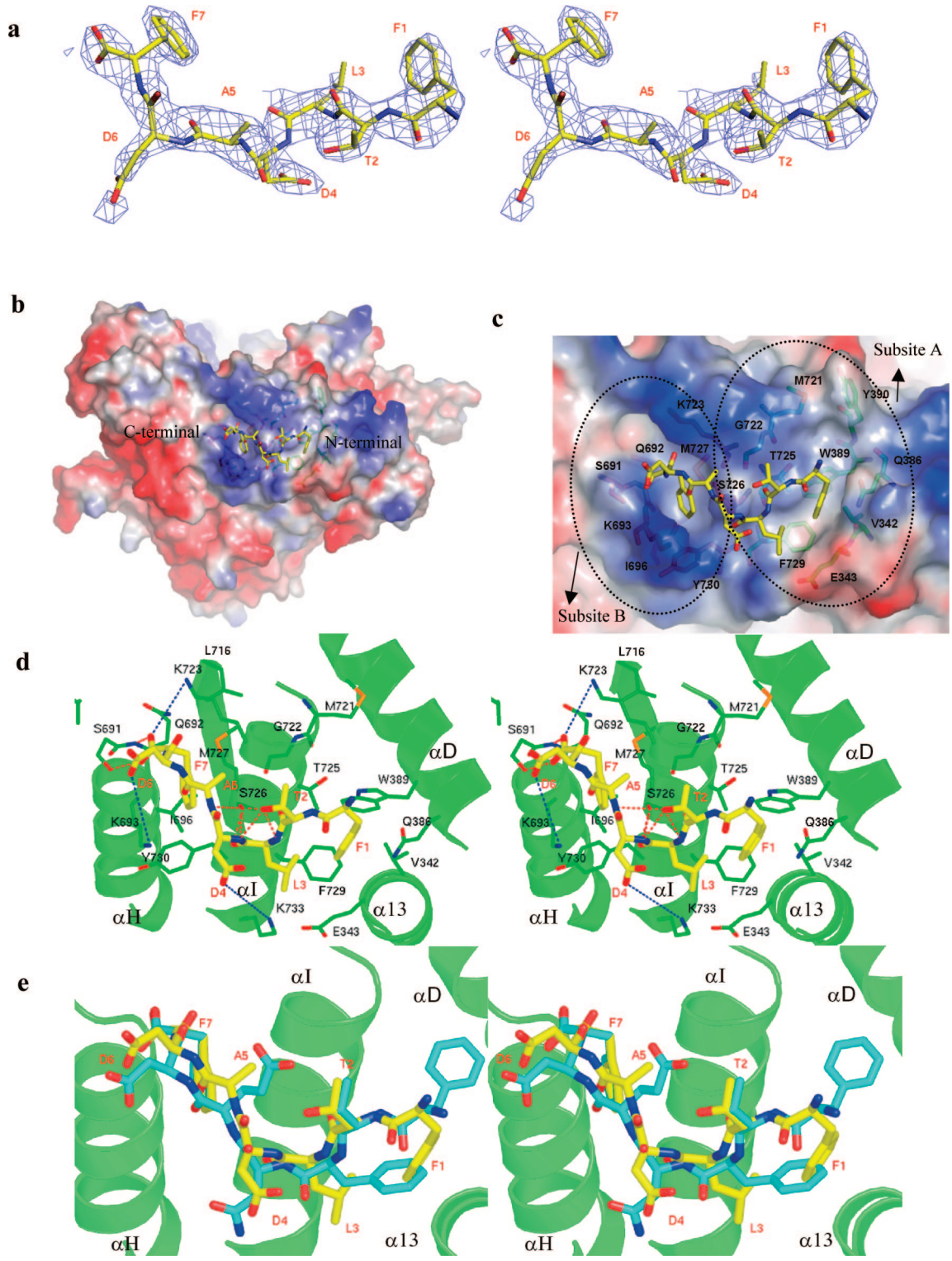

Figure 1. ScR1−P7 complex. (a) Stereo view of the $2F_o - F_c$ difference Fourier electron density map contoured at 1 σ, displayed in blue. The peptide is color coded as carbon yellow, nitrogen blue and oxygen red. (b−c) The electrostatic potential surface showing the R2 binding site on R1. Left: Overall electrostatic surface of the protein. Right: A zoom view of the electrostatic surface of the P7 binding site that includes pockets A and B. Red indicates negative surface charges, blue indicates positive surface charges, and gray represents uncharged surfaces. Peptide residues (carbon atoms, yellow; oxygens, red; and nitrogens, blue). (d) Stereo pictures of the interactions between ScR1 and P7. Hydrogen bonds are drawn in red dash lines and salt-bridges drawn in blue. (e) ScR2 peptide superimposed on P7. The peptide is drawn from right to left. P7 is drawn in yellow and ScR2 peptide in cyan. Only P7 is labeled in red. Nearby helices are drawn from the P7−R1 complex (green).

Bound P7 displays strong amphipathic features, as was observed with the ScR2 peptide. The P7 side chains of F^1, L^3, and F^7 (corresponding to F^1, F^3, and F^7 in the ScR2 heptapeptide) point toward the interior of the ScR1 molecule, providing most of the hydrophobic binding energy (Figure 1e). In contrast, the side chains of D^4 and D^6 in P7 (corresponding to N^4 and D^6 in the ScR2 heptapeptide) and the C-terminal carboxylate are partially solvent exposed and bind at a complementary positively charged surface (Figure 1e). At the N-terminus of the ScR2 heptapeptide, F^1 and F^3, which are contiguous, bind

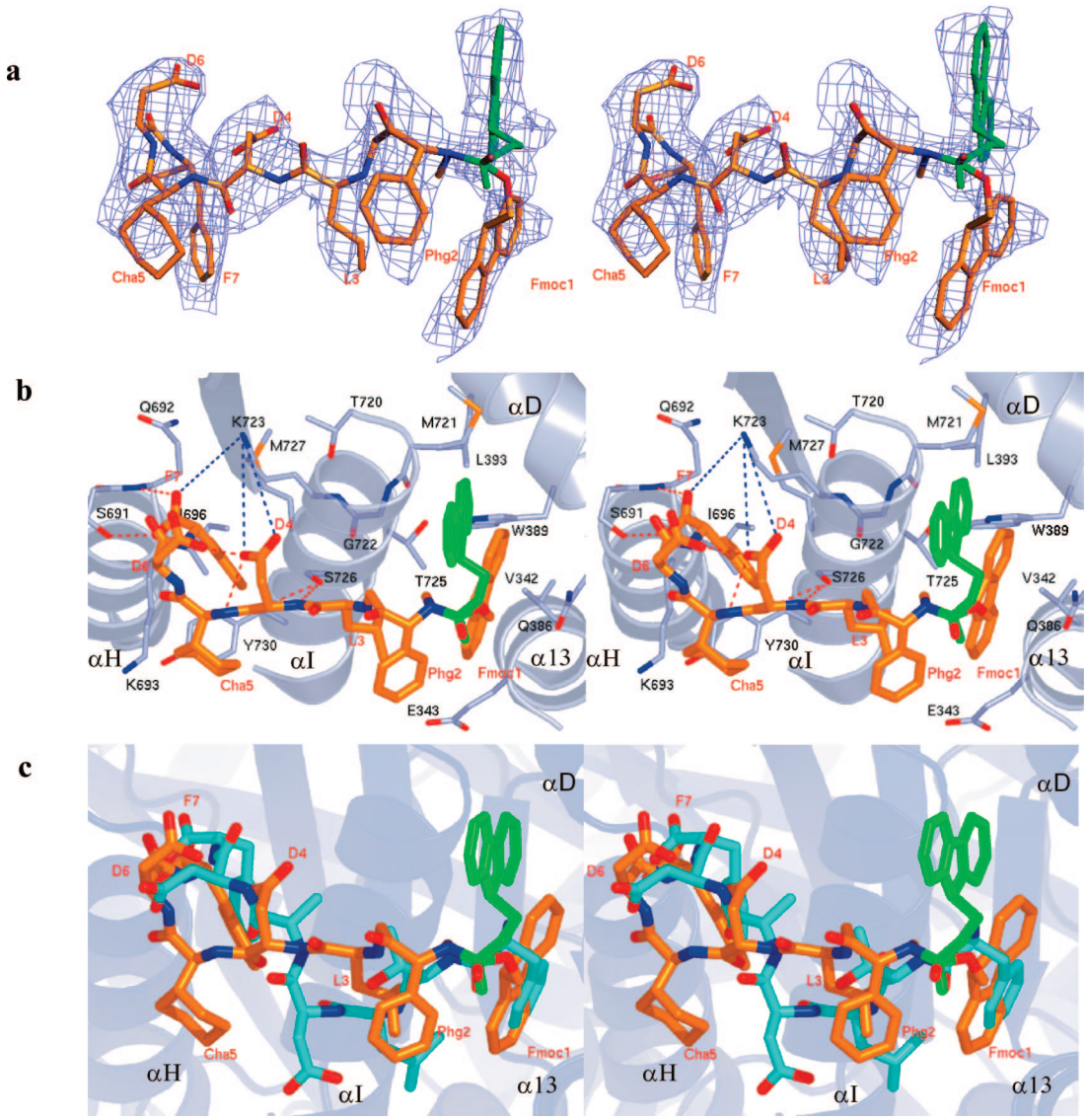

Figure 2. ScR1−P6 complex. (a) Stereo view of the $2F_o - F_c$ difference Fourier map contoured at 0.7σ, displayed in blue. The peptide is color coded as carbon orange, nitrogen blue, and oxygen red. (b) Stereo view showing the interactions between R1 and P6. (c) P6 superimposed with P7. Carbon atoms for P7 (cyan) and P6 (orange) and nearby helices are drawn from the P7−R1 complex (blue). The alternative conformation of the P6 Fmoc group is shown in green in all the figures. Only P6 is labeled in red.

by extending further along the surface of subsite A compared to P7, making several hydrophobic interactions (Figure 1e). In P7, the aromatic side-chain of F^1 points towards the interior of the pocket and makes contact with V342, E343, Q386, W389, T725, and T729, while the corresponding residue, F^1 of the ScR2 peptide, binds in an almost perpendicular manner, pointing towards αD and making contact with Q386, W389, Y390, L393, M721, and T725. The differing aromatic conformations are due to steric effects resulting from substitution at position 3 of Phe in ScR2pep for Leu in P7.

Structure of ScR1−P6 Peptidomimetic Complex. Although P6 inhibits mRR and ScRR with IC_{50} values that are 5-fold and 12-fold lower, respectively, than those determined for P7 (see Table 1), the $2F_o - F_c$ electron density for P6 bound to ScR1 is slightly weaker than that observed for P7 (see Figure 1a versus Figure 2a). This may be due to the low solubility of P6, which could limit the amount of compound soaking into the crystal, hence lowering its occupancy when binding to ScR1. However, the $2F_o - F_c$ difference Fourier electron density map clearly shows that the P6 peptide binds ScR1 with a partially extended conformation (Figure 2b), lacking the reverse turn found in ScR1-bound P7 or ScR2 peptide (Figure 2c). There are also main chain conformational differences between positions 4 and 6. We attribute the altered mode of P6 binding to the substitution of nonstandard residues ^{1}Fmoc(Me), Phg, and Cha at positions 1, 2, and 5, respectively. The ScR1-bound structures of P7 and P6 superpose with an rmsd of 1.88 Å, further demonstrating their main chain conformational differences (Figure 2c).

Previously, we had proposed that the addition of the Fmoc group at the N-terminus would improve binding due to the contributions of the hydrophobic interactions made with mR1 at the A subsite.[12,18] Although the resolution of the P6 structure (2.5 Å) is insufficient to conduct occupancy refinement, we clearly see electron density for two conformations (see Figure 2A). On the basis of comparisons of B-factors, the Fmoc conformation binding at the hydrophobic subsite A (major conformation, Figure 2 drawn in orange) is likely to have the greater occupancy, while the minor conformation partially points to solvent (Figure 2 drawn in green). The major conformation of Fmoc makes several intramolecular and intermolecular hydrophobic interactions (Figure 2b). One of the six-membered

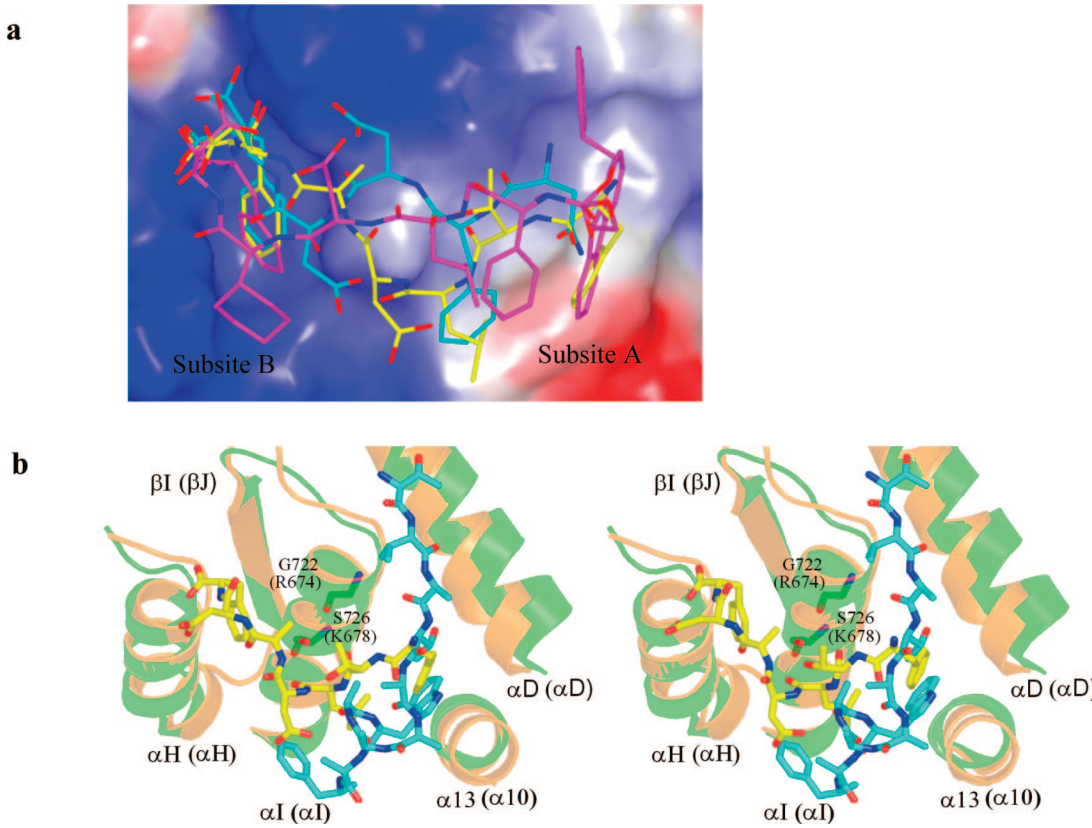

Figure 3. (a) Structural comparison of P7, P6, and ScR4 peptide binding to ScR1. Carbon atoms for P7 (yellow), P6 (magenta), and ScR4 (cyan). Surface is drawn from the ScR1−P6 complex. (b) Stereo view of P7 superposed with *S. typhimurium* R2. *S. typhimurium* is drawn in orange and its R2pep in cyan, while ScR1 in green and P7 is in yellow. Labels for *S. typhimurium* R1 are shown in parenthesis.

rings of Fmoc binds ScR1 almost identically to the F^1 side chain of the P7 inhibitor, while the second six-membered ring makes additional hydrophobic interactions with the indole ring of W389 and the side-chain of L393 (see Supporting Information Table 1). The alternate minor conformation of Fmoc makes interactions with M721 and G722. These additional hydrophobic interactions are likely to be at least partly responsible for the enhanced affinity of P6 vs P7 for ScR1.

The phenylglycine (Phg) residue at position 2 forms intramolecular contacts with the major conformation of Fmoc and L^3. Additionally, the L^3 residue contacts the major conformation of Fmoc, G722, T725, and S726 of the protein and partially binds in the A subsite. The carboxyl group of D^4 also makes a weak hydrogen bond with the Cha^5 amide nitrogen, interacts with the D^6 side chain, and makes an ion pair interaction with K723 (see Supporting Information Table 1). The Cha side chain at position five makes contact with K693 only. Comparing P7 and P6 structures, the Cα atoms of D^6 are 2.6 Å apart. The carboxyl group of D^6 in P6 points towards the protein and makes an intramolecular hydrogen bond with the side chain of D^4 that P7 does not make due to altered side chain conformations. However, the aromatic F^7 residue and the terminal carboxylate bind almost identically within subsite B in both structures (Figure 2b).

Comparison of ScR4 Peptide Binding with P7 and P6 Binding to ScR1. As reported earlier,[17] ScR4pep (^{2}NFDDDF^7) binds to ScR1 somewhat differently than ScR2pep. When the ScR1-bound forms of P7 and P6 are each superposed with the corresponding form of ScR4pep, the backbone rmsds are 1.86 and 0.97 Å, respectively, indicating that P6 has greater conformational similarity to ScR4pep than does P7 (Figure 3a). This greater similarity is clearest at subsite A, within which the side chains of N^2 and F^3 of ScR4pep overlap with the Fmoc and Phg of P6, respectively. In contrast, in P7 only F^1 bound at subsite A overlaps with N^2 of ScR4pep. However, the opposite trend is found at subsite B. Here, the conserved ^{6}DF^7 residues in P7 and ScR4pep superpose perfectly, whereas only the F^7residue of P6 overlaps with ScR4pep. Lastly, although both ScR4pep and P7 have a reverse turn that is lacking in P6, the reverse turns run in opposite directions. Interestingly, the loss of solvent accessibility (SA) is greater for P6 binding to ScR1 (422.8 Å^2) than for P7 binding to ScR1 (384.8 Å^2), consistent with the higher inhibitory potency (Table 1) and binding affinity for mR1 (26) of P6 vs P7.

Comparison of the Mode of R1−R2 Binding between Eukaryotes and Prokaryotes. Here we show that the P7 mammalian inhibitor binds to ScR1 with a conformation similar to that of the ScR2 peptide (Figure 1e). Similarly, in the recent 4 Å crystal structure of the R1−R2 holocomplex from *Salmonella typhimurium* (S. typhimurium),[19] the R2 C-terminus of S. typhimurium (StR2pep) was shown to bind to S. typhimurium R1 (StR1) analogously to EcR2 peptide binding to EcR1. However, the modes of R2 C-terminal peptide binding to eukaryotic vs prokaryotic R1 diverge markedly from one another, accounting for the observations that *E. coli*-based R2 oligopeptides do not inhibit mRR activity and vice versa.[20]

Superposition of the StR1−StR2pep and ScR1−P7 structures (Figure 3b) reveals that subsite A in ScR1 only partially overlaps with the large hydrophobic cleft consisting of residues from αI, α13 (α10 in *S. typhimurium*), and αD in StR1. Moreover, the cavities in the two prokaryotes each have a larger accessible area compared to subsite A, providing a compelling rationale for why an EcR2 20-mer peptide binds EcR1 with a higher affinity (K, 20 μM) than an EcR2 octapeptide (K_i, 370 μM),[21]

whereas increasing the length of the P7 peptide beyond a heptamer has little effect on affinity.[11] In addition, predicted secondary structures[22] of R2 C-termini indicate that prokaryotic sequences are much more likely to form helices, capable of interacting with helices α13, αI, and αD, than eukaryotic sequences (data not shown).

Even more strikingly, subsite B, which accommodates D^6 and F^7 of P7, and is located between αH, βI, and the N-terminal half-of αI, has virtually no steric overlap with the region of EcR1 or StR1, consisting of α13, α22, and the C-terminal half-of αI, that serves as the binding site for the ultimate EcR2 or StR2 C-terminal residues (Figure 3b). This major difference may largely be accounted for by the significant divergence in sequence at the hydrophobic cleft between eukaryotes and prokaryotes (see Supporting Information Figure 2). In particular, residues R674 and K678 within αI in StR1 (corresponding to Q712 and K716 in EcR1) will sterically interfere with the StR2 peptide binding to StR1 in the manner of ScR2 peptide binding to ScR1 (Figure 3b). In ScR1 and mR1, such interference is not seen because the corresponding residues in αI are G722 and S726 and G718 and S722, respectively. Moreover, in the ScR1−P7 complex, both S726 and G722 are involved in key hydrogen bonds and van der Waals interactions with P7.

Implications for Drug Design. The structures and structural models presented in this work provide a promising basis for efforts to design new peptide and peptidomimetic ligands for hR1 with affinities and RR inhibitory potencies that will exceed those of P6. Such efforts will exploit the flexibility in the eukaryotic R1 binding site, evident from the different conformations adopted by (i) P7/ScR2pep, (ii) P6, and (iii) ScR4pep and seek to maximize the SA loss resulting from enhanced interactions with subsites A and B and with the interaction surface in R1 that connects these subsites. As one example, we are currently exploring the possibility of replacing the F^1 and L^3 residues of P7, which bind ScR1 contiguously within subsite A, with a nonpeptide hydrophobic macrocyclic group that will optimize interaction at this subsite. A similar strategy has been successfully pursued by Novartis in developing the hypertensive renin inhibitor Aliskiren, currently in phase III trials, which involved replacement of the P^1 (L) and P^3 (F) residues that bind within a large hydrophobic pocket (32−34). Moreover, all three modes of binding defined by these structures provide templates for designing cyclic peptidomimetic molecules that connect both the sites.

Experimental Section

Peptide Synthesis. P7 with sequence Ac−^{1}FTLDADF^{7}and peptidomimetic P6 with sequence ^{1}Fmoc(Me)PhgLDChaDF^7 were synthesized and purified as described in ref 23.

Expression and Purification of 6X-His-ScR2/R4. The ScR2/R4 subunits were prepared from BL21(DE3) Codon Plus RIL bacteria transformed with plasmid pET21. All purification steps were performed at 4 °C. Complete Protease Inhibitor tablets (EDTA free) (1/25 mL buffer) were added to all buffers prior to use. Supernatant prepared by French press opening of bacterial cells was loaded onto a Ni-NTA resin in Buffer A (50 mM potassium phosphate pH 7.4; 100 mM KCl) and, following column washing by Buffer B (Buffer A + 10 mM Imidazole), 6X-His-ScR2/R4 was eluted with Buffer C (Buffer A + 100 mM imidazole), dialyzed against Buffer A, and flash frozen in aliquots.

ScR1 Purification and Crystallization of ScR1 in Complex with Mammalian R2 Inhibitors. ScR1 was produced and purified as described previously[16] and crystallized from a reservoir solution containing 20−25% PEG 3350, 0.2 M NaCl, and 100 mM Hepes, pH 7.5. The ScR1 protein concentration was 20 mg/mL, which was in a 0.1 M Hepes pH 7.5 buffer with 20 mM TTP, 5% glycerol, 5mM DTT, 0.1 M KCL, and 25 mm $MgCl_2$. Crystals were incubated for 4 h in reservoir solution containing saturated P7 and P6. Subsequently, crystals were soaked in 25% PEG 3350, 0.2 M NaCl, and 100 mM Hepes, pH 7.5, supplemented with 15% glycerol and cryo-cooled.

Table 2. Data Collection and Refinement Statistics for Mammalian−R1 Inhibitor Complex Structures

	P7−R1 complex	P6−R1 complex
	Data Collection	
space group	$P2_12_12$	$P2_12_12$
cell dimensions *a*, *b*, *c* (Å)	107.95, 117.00, 63.87	107.79, 116.57, 63.64
wavelength (Å)	0.90020	0.90020
resolution (Å)	50.0−2.6	50.0−2.5
unique/total reflections	24929/163941	27055/125484
R_{sym} (%)[a]	8.1 (45.9)	7.4 (46.1)
$I/(I)$ [a]	21.5 (2.1)	18.8 (2.4)
completeness (%)[a]	96.5 (82.4)	98.3 (92.4)
redundancy [a]	6.6 (5.8)	4.7 (3.8)
	Refinement	
resolution (Å)	50−2.6	50.0−2.5
no. reflections	23621	25564
R_{work}/R_{free}[b]	0.196/0.251	0.219/0.292
no. atoms		
protein	5297	5229
ligand/ion	58[c]	102[d]
water	72	92
B-factors		
protein	36.8	40.63
ligand/ion	57.4	72.3
water	34.0	37.3
rms deviations		
bond lengths (Å)	0.009	0.006
bond angles (deg)	1.46	1.42

[a] Highest resolution shell is shown in parentheses. [b] R_{work} and $R_{free} = \sum||F_o| - |F_c||/\sum|F_o|$, where F_o and F_c are the observed and calculated structure factor amplitudes. For the calculation of R_{free}, 10% of the reflection data were selected and omitted from refinement. [c] The ligand/ion is P7 peptide. [d] The ligand/ion is glycerol and P6 peptide.

Structure Determination. X-ray data were collected at BioCARS beamline BMC14 (APS, USA) and processed with HKL2000[24] (see Table 2). Because the complex crystals were isomorphous to native ScR1 with one monomer in the asymmetric unit (Protein Data Bank code 2CVS), the initial structures were directly determined by difference Fourier techniques. The F_o-F_c difference Fourier electron density maps clearly showed the bound inhibitors, which were modeled using the program O.[25] Subsequently, restrained refinement implemented in REFMAC5[26] and PHENIX[27,28] interspersed with model building was conducted for several cycles until there was no further improvement in the R_{free} (see Table 2). All figures of the molecules were prepared with Pymol.[29]

Assay of ScRR Activity. Assays were conducted as previously described for mRR,[23] except that the total ScR2/R4 concentration was 1.5 μM, GDP concentration was increased from 150 to 300 μM, and the reaction time was decreased from 20 to 10 min. Under these conditions, the assay was proportional to ScR1 concentration in the range 0.0−0.9 μM.

Acknowledgment. We thank the members of the BMC beamline at BioCARS at APS with data collection. We thank Dr. Brad Bennett for proof reading this manuscript. This work was supported by NIH grant numbers 2R01CA100827-04A1 and 2R01CA058567-09A1 and the Elisa Pardee foundation.

Supporting Information Available: A table of comparison of the interactions of the P7, P6, and ScR2 Peptide with ScR1, a stereo view of the structural comparison of ScR2, ScR4, and EcR2 peptide binding, and the sequence comparison of the binding site forming the hydrophobic cleft on *S. typhimurium*, *E.coli,* yeast and mouse R1 and also the R2 C-terminals from *S. typhimurium*, *E. coli*, yeast, and mouse are provided. This material is available free of charge via the Internet at http://pubs.acs.org.

References

(1) Stubbe, J. Ribonucleotide reductases: the link between an RNA and a DNA world. *Curr. Opin. Struct. Biol.* **2000**, *10*, 731–736.

(2) Bollinger, J. M., Jr.; Edmondson, D. E.; Huynh, B. H.; Filley, J.; Norton, J. R.; Stubbe, J. Mechanism of assembly of the tyrosyl radical-dinuclear iron cluster cofactor of ribonucleotide reductase. *Science* **1991**, *253*, 292–298.

(3) Fontecave, M.; Eliasson, R.; Reichard, P. Enzymatic regulation of the radical content of the small subunit of *Escherichia coli* ribonucleotide reductase involving reduction of its redox centers. *J. Biol. Chem.* **1989**, *264*, 9164–70.

(4) Sommerhalter, M.; Voegtli, W. C.; Perlstein, D. L.; Ge, J.; Stubbe, J.; Rosenzweig, A. C. Structures of the yeast ribonucleotide reductase Rnr2 and Rnr4 homodimers. *Biochemistry* **2004**, *43*, 7736–7742.

(5) van der Donk, W. A.; Yu, G.; Silva, D. J.; Stubbe, J.; McCarthy, J. R.; Jarvi, E. T.; Matthews, D. P.; Resvick, R. J.; Wagner, E. Inactivation of ribonucleotide reductase by (*E*)-2′-fluoromethylene-2′-deoxycytidine 5′-diphosphate: a paradigm for nucleotide mechanism-based inhibitors. *Biochemistry* **1996**, *35*, 8381–8391.

(6) Szekeres, T.; Fritzer-Szekeres, M.; Elford, H. L. The enzyme ribonucleotide reductase: target for antitumor and anti-HIV therapy. *Crit. Rev. Clin. Lab. Sci.* **1997**, *34*, 503–28.

(7) Mayhew, C. N.; Phillips, J. D.; Greenberg, R. N.; Birch, N. J.; Elford, H. L.; Gallicchio, V. S. In vivo and in vitro comparison of the short-term hematopoietic toxicity between hydroxyurea and trimidox or didox, novel ribonucleotide reductase inhibitors with potential anti-HIV-1 activity. *Stem Cells* **1999**, *17*, 345–356.

(8) Yang, F. D.; Spanevello, R. A.; Celiker, I.; Hirschmann, R.; Rubin, H.; Cooperman, B. S. The carboxyl terminus heptapeptide of the R2 subunit of mammalian ribonucleotide reductase inhibits enzyme activity and can be used to purify the R1 subunit. *FEBS Lett.* **1990**, *272*, 61–4.

(9) Fisher, A.; Laub, P. B.; Cooperman, B. S. NMR structure of an inhibitory R2 C-terminal peptide bound to mouse ribonucleotide reductase R1 subunit. *Nat. Struct. Biol.* **1995**, *2*, 951–5.

(10) Pellegrini, M.; Liehr, S.; Fisher, A. L.; Laub, P. B.; Cooperman, B. S.; Mierke, D. F. Structure-based optimization of peptide inhibitors of mammalian ribonucleotide reductase. *Biochemistry* **2000**, *39*, 12210–5.

(11) Fisher, A.; Yang, F. D.; Rubin, H.; Cooperman, B. S. R2 C-terminal peptide inhibition of mammalian and yeast ribonucleotide reductase. *J. Med. Chem.* **1993**, *36*, 3859–62.

(12) Pender, B. A.; Wu, X.; Axelsen, P. H.; Cooperman, B. S. Toward a rational design of peptide inhibitors of ribonucleotide reductase: structure−function and modeling studies. *J. Med. Chem.* **2001**, *44*, 36–46.

(13) Liehr, S.; Barbosa, J.; Smith, A. B., III. Cooperman, B. S. Synthesis and biological activity of cyclic peptide inhibitors of ribonucleotide reductase. *Org. Lett.* **1999**, *1*, 1201–1204.

(14) Uhlin, U.; Eklund, H. Structure of ribonucleotide reductase protein R1. *Nature* **1994**, *370*, 533–539.

(15) Cooperman, B. S.; Gao, Y.; Tan, C.; Kashlan, O. B.; Kaur, J. Peptide inhibitors of mammalian ribonucleotide reductase. *Adv. Enzyme Regul* **2005**, *45*, 112–115.

(16) Xu, H.; Faber, C.; Uchiki, T.; Fairman, J. W.; Racca, J.; Dealwis, C. Structures of eukaryotic ribonucleotide reductase I provide insights into dNTP regulation. *Proc. Natl. Acad. Sci. U.S.A.* **2006**, *103*, 4022–4027.

(17) Xu, H.; Faber, C.; Uchiki, T.; Racca, J.; Dealwis, C. Structures of eukaryotic ribonucleotide reductase I define gemcitabine diphosphate binding and subunit assembly. *Proc. Natl. Acad. Sci. U.S.A.* **2006**, *103*, 4028–4033.

(18) Gao, Y.; Liehr, S.; Cooperman, B. S. Affinity-driven selection of tripeptide inhibitors of ribonucleotide reductase. *Bioorg. Med. Chem. Lett.* **2002**, *12*, 513–515.

(19) Uppsten, M.; Farnegardh, M.; Domkin, V.; Uhlin, U. The first holocomplex structure of ribonucleotide reductase gives new insight into its mechanism of action. *J. Mol. Biol.* **2006**, *359*, 365–377.

(20) Cosentino, G.; Lavallee, P.; Rakhit, S.; Plante, R.; Gaudette, Y.; Lawetz, C.; Whitehead, P. W.; Duceppe, J. S.; Lepine-Frenette, C.; Dansereau, N.; Guilbault, C.; Langelier, Y.; Gaudreau, P.; Thelander, L.; Guindon, Y. Specific inhibition of ribonucleotide reductases by peptides corresponding to the C-terminal of their second subunit. *Biochem. Cell Biol.* **1991**, *69*, 79–83.

(21) Climent, I.; Sjoberg, B. M.; Huang, C. Y. Carboxyl-terminal peptides as probes for *Escherichia coli* ribonucleotide reductase subunit interaction: kinetic analysis of inhibition studies. *Biochemistry* **1991**, *30*, 5164–5171.

(22) Pollastri, G.; Przybylski, D.; Rost, B.; Baldi, P. Improving the prediction of protein secondary structure in three and eight classes using recurrent neural networks and profiles. *Proteins* **2002**, *47*, 228–235.

(23) Tan, C.; Gao, Y.; Kaur, J.; Cooperman, B. S. More potent linear peptide inhibitors of mammalian ribonucleotide reductase. *Bioorg. Med. Chem. Lett.* **2004**, *14*, 5301–5304.

(24) Minor, W.; Tomchick, D.; Otwinowski, Z. Strategies for macromolecular synchrotron crystallography. *Struct. Fold Des.* **2000**, *8*, R105–R110.

(25) Jones, T. A.; Zou, J. Y.; Cowan, S. W. Kjeldgaard. Improved methods for building protein models in electron density maps and the location of errors in these models. *Acta Crystallogr., Sect. A: Found. Crystallogr.* **1991**, *47*, 110–119.

(26) CCP4. Collaborative Computing Project in protein crystallography. In *SERC*,Daresbury Laboratory:Warrington, UK, 1985.

(27) Adams, P. D.; Grosse-Kunstleve, R. W.; Hung, L. W.; Ioerger, T. R.; McCoy, A. J.; Moriarty, N. W.; Read, R. J.; Sacchettini, J. C.; Sauter, N. K.; Terwilliger, T. C. PHENIX: building new software for automated crystallographic structure determination. *Acta Crystallogr., Sect. D: Biol. Crystallogr.* **2002**, *58*, 1948–1954.

(28) Adams, P. D.; Gopal, K.; Grosse-Kunstleve, R. W.; Hung, L. W.; Ioerger, T. R.; McCoy, A. J.; Moriarty, N. W.; Pai, R. K.; Read, R. J.; Romo, T. D.; Sacchettini, J. C.; Sauter, N. K.; Storoni, L. C.; Terwilliger, T. C. Recent developments in the PHENIX software for automated crystallographic structure determination. *J. Synchrotron Radiat.* **2004**, *11*, 53–55.

(29) DeLano, W. L. *The Pymol Molecular Graphics System*; DeLano Scientific: San Carlos, 2002.

(30) Chabes, A.; Domkin, V.; Thelander, L. Yeast Sml1, a protein inhibitor of ribonucleotide reductase. *J. Biol. Chem.* **1999**, *274*, 36679–36683.

JM800350U